JOURNAL OF CATALYSIS 113, 220–235 (1988)

Formation of Pt Particles in Y-Type Zeolites

The Influence of Coexchanged Metal Cations

M. S. TZOU, B. K. TEO,* AND W. M. H. SACHTLER[1]

*Ipatieff Laboratory, Department of Chemistry, Northwestern University, Evanston, Illinois 60208, and *Department of Chemistry, University of Illinois, Chicago, Illinois 60204*

Received January 1, 1988; revised March 29, 1988

Samples of platinum, supported on NaY, HNaY, and M/NaY ($M = Ca^{2+}$, La^{3+}, or Fe^{2+}), have been studied by temperature-programmed reduction (TPR), desorption (TPD), and extended X-ray absorption fine structure (EXAFS) to investigate the mechanism of the formation of Pt particles and the influence of H^+ and added metal cations on it. Size and location of Pt particles in a zeolite matrix were found to be strongly dependent on the distribution of Pt ions between the supercages and the sodalite cages, which is controlled by the calcination temperature (T_c) prior to the reduction. At low T_c (e.g., 360°C), the majority of the Pt^{2+} ions are in the supercages; after reduction small particles (5–10 Å) are formed which are also located in the supercages. This is also true for Pt/Y with or without coexchanged multivalent cations. The Pt^0–O^{2-} distance is 2.65 Å as derived from the k^1-weighted EXAFS functions. At medium T_c (e.g., 450°C), the Pt^{2+} ions are distributed between supercages and sodalite cages. In this case, the Pt^{2+} ions in the supercages are reduced first to form small particles which become nucleation sites for Pt^0 atoms leaving the sodalite cages above 400°C. Eventually, these Pt particles can become larger than the supercages. At high T_c (e.g., 550°C), most Pt^{2+} ions migrate to sodalite cages and require a high reduction temperature (T_r). The reduced Pt^0 atoms then migrate from sodalite cages to supercages, and in the absence of nucleation sites they finally coagulate on the external surface of the zeolite crystals to form large Pt particles. However, the presence of coexchanged multivalent cations, e.g., Fe^{2+}, which can effectively block sodalite cages and hexagonal prisms, thus forcing Pt^{2+} ions to stay in supercages, can prevent the formation of large particles on the external surface of zeolites even at high T_c. The evolution of hydrogen at $T_{max} = 450$°C, caused by oxidative reaction of Pt^0 atoms with hydroxyl groups during TPD, as indicated by FTIR, can be used to determine the presence of Pt in sodalite cages.

1. INTRODUCTION

In principle, transition metal/zeolite catalysts are capable of combining the catalytic qualities of highly dispersed metals of fairly uniform particle size with the stereospecificity imposed by the three-dimensional geometry of zeolites. They can also act as bifunctional catalysts, if the zeolite is used in its acidic mode (*1*). Studies of transition/metal zeolite combinations by Rabo, Boudart, Gallezot, Jacobs, Delafosse, and others have provided important information (*2–10*). At present, the major application is in hydrocracking (*11*). Major problems still exist in the preparation of catalysts with uniform particle size of highly dispersed metals, the dispersion maintenance of these systems under severe reaction conditions, and their *in situ* rejuvenation.

The present paper focuses on the first of these problems. We have studied the formation mechanism of Pt particles in zeolites Y, focusing attention on the effects of calcination conditions of the $Pt(NH_3)_4^{2+}$-containing zeolite on the temperature requirement for its subsequent reduction, and

[1] To whom all correspondence should be addressed.

0021-9517/88 $3.00

the effect of these parameters on the size and location of the ultimate particles (*12*). We further studied the effects of auxiliary ions, which had been exchanged into the zeolite, on the reduction of platinum. Recently, we found that exchanging Fe^{2+} ions into NaY dramatically decreases the size of Pt particles in the same zeolite, when calcined at high temperatures (*13*). Also the reducibility of Ni is significantly increased, if Mn^{2+} or Cr^{3+} ions are exchanged in the zeolite prior to Ni ion exchange (*14*). Likewise, Tri *et al.* reported that the size of Pt particles was decreased from 10 to 8 Å in the presence of Ce^{3+} ions (*15*). In addition to enhancing the reducibility of the catalytic metal, these coexchanged ions can also affect its catalytic activity in a favorable way (*3, 16*). In the present paper, TPR (temperature-programmed reduction), TPD (temperature-programmed desorption), FTIR (Fourier transform infrared spectroscopy), and EXAFS (extended X-ray absorption fine structure), are combined to study the effect of various cations, e.g., Fe^{2+}, Ca^{2+}, La^{3+}, and H^+, on the formation of Pt particles.

2. EXPERIMENTAL

2.1. Catalyst Preparation

The catalysts of interest in this investigation contain both calcined and reduced platinum supported in zeolite NaY, or *M*/NaY, where *M* is Fe^{2+}, Ca^{2+}, or La^{3+}. The zeolite was kindly donated by Union Carbide, the label indication being LZ-Y52, Lot No. 968083061080-S-9. A Pt/HNaY sample which was prepared from HNaY (LZ-Y72, Lot No. 966484060291-S-8) was also studied. CaNaY and LaNaY were prepared by ion exchange of 200 ppm $Ca(NO_3)_2$ or $La(NO_3)_3$ solutions with NaY (1 g/100 ml). The zeolites were then heated *in vacuo* by raising the temperature from 25 to 400°C over a period of 12 h and kept at 400°C for another 12 h. The dehydrated CaNaY and LaNaY as well as NaY and HNaY (LZ-Y72) were then exchanged with a 200 ppm $Pt(NH_3)_4Cl_2$ solution at 80°C for 12 h. The preparation procedures for FeNaY and $Pt(NH_3)_4$/FeNaY were described before (*13*). The FeNaY was also dehydrated *in vacuo* prior to exchange with a $Pt(NH_3)_4Cl_2$ solution. The loadings of platinum in these zeolites range from 7.5 to 14.2 wt%, which correspond approximately to 4.8 to 9.4 Pt atoms per unit cell or 0.6 to 1.2 Pt atoms per supercage. The compositions of the dried metal/zeolite catalysts are listed in Table 1.

2.2 Catalyst Pretreatment Procedures

The standard calcination procedures for the samples, that were studied by temperature-programmed reduction, desorption, and extended X-ray absorption fine structure consisted of thermal treatment from 25 to 360, 450, or 550°C in O_2 at a heating rate of 0.5°C/min. The samples were then kept at 360, 450, or 550°C in O_2 for 2 h and further in Ar for 1 h before being cooled to room temperature under flowing Ar. In order to prevent autoreduction of Pt by decomposing NH_3, a high O_2 flow rate of 1000 ml per minute per gram catalyst was used, following suggestions by Dalla Betta and Boudart (*3*) and Gallezot *et al.* (*4*). In this paper the catalysts treated at 360 or 550°C are designated Pt/Y(360) and Pt/Y(550), respectively. The sample color after calcination is greenish-black for Pt/Y(360) and light gray for Pt/Y(550). In general, a Pt/Y sample of 0.12 g suffices for

TABLE 1

The Chemical Composition of Pt Containing Y-Type Zeolite Catalysts

Catalysts	wt% Pt	wt% *M*[a]
Pt/NaY	8.6	
Pt/HNaY	7.5	
Pt/FeNaY	14.2	3.67
Pt/CaNaY	9.6	2.75
Pt/LaNaY	10.8	10.5

[a] *M* is Fe, Ca, or La.

each TPR and TPD experiment and 0.25 g for EXAFS.

2.3. TPR and TPD Experimental Procedures

The calcined Pt/Y catalysts were cooled to −80°C in Ar; for TPR experiments the gas flow was then changed to 5% H_2/Ar at −80°C, whereas for TPD a gas flow of pure Ar was used. The flow rate was 30 ml/min for either gas, and the heating rate 8°C/min. A detailed description of the apparatus was given in a previous paper (*17*). H_2 gas injections were used to quantify the consumption and desorption or evolution of hydrogen in TPR and TPD. All gases used in the pretreatment and the TPR or TPD procedures (Ar, O_2, and 5% H_2/Ar) were ultrapure grade from Matheson. The TPR/TPD apparatus has an extremely small dead volume and is interfaced with a personal computer. The quantity of hydrogen that is consumed in TPR or released in TPD is determined reproducibly within 10%; the precision in the temperature of a TPR or TPD peak is about 5°C.

2.4. Infrared Spectroscopy

Infrared spectra of Pt/NaY were recorded by a Nicolet-60SX spectrometer with a resolution of 4 cm^{-1}. The sample cell was similar to that used by Tessier-Youngs *et al.* for the investigations of iron complexes supported on Al_2O_3 (*18*). The pellet, which was pressed (8 mg/7 mm diameter) after the calcination of Pt/NaY at 550°C, was dehydrated in Ar at 550°C in a sample tube, and this was followed by reduction (TPR up to 400°C) and desorption (TPD up to 550°C).

2.5. X-Ray Absorption Measurements

For the EXAFS studies, the catalysts placed in a pretreatment tube were calcined as described above and then continuously heated in Ar for 1 h, H_2 for 2 h, and again Ar for 1 h at 360 or 550°C. After cooling to room temperature, the calcined or reduced zeolite samples were transferred to an aluminum holder in Ar without being exposed to air. The sample holder possessing two Kapton films (500-μm thickness) as X-ray windows was sealed in Ar to be ready for X-ray absorption experiments at room temperature (*19*). The X-ray absorption measurements in the range of the Pt L_{III}-edge (11.5 keV) were made at the C1 and C2 stations of the Cornell High Energy Synchrotron Source (CHESS).

2.6. EXAFS Data Analysis

The raw EXAFS data in energy space ($\ln(I_0/I)$ vs E) were reduced to the photoelectron wave vector (k) space as described elsewhere (*19, 20*), with E_0 = 11.5 eV, where $k = [2m(E - E_0)/\hbar^2]^{1/2}$. The resulting $k^1 \cdot \chi(k)$ or $k^3 \cdot \chi(k)$ functions vs k data and the corresponding Fourier transforms were obtained in the same way as before (*19, 20*). For the purpose of curve fitting (CF), the high-frequency noise was removed by a Fourier filtering technique. The resulting filtered data are fitted with theoretical phase and amplitude functions.

3. RESULTS

3.1. Temperature-Programmed Reduction and Desorption

The TPR profiles, starting from −80 to 550°C with a heating rate of 8°C/min are shown in Fig. 1 for Pt/NaY calcined at 360, 450, and 550°C. It is clear that the reduction temperature increases with calcination temperature. Integration of the area under each profile shows that two H atoms are consumed per Pt ion, which implies that Pt remains in the divalent state also after calcination. The hydrogen TPD shown by the solid curves of Figs. 1d–1f reveals that the H/Pt ratios for these samples are 1.10, 0.60, and 0.30 ± 0.10, respectively. If reduction was interrupted at 400°C when the

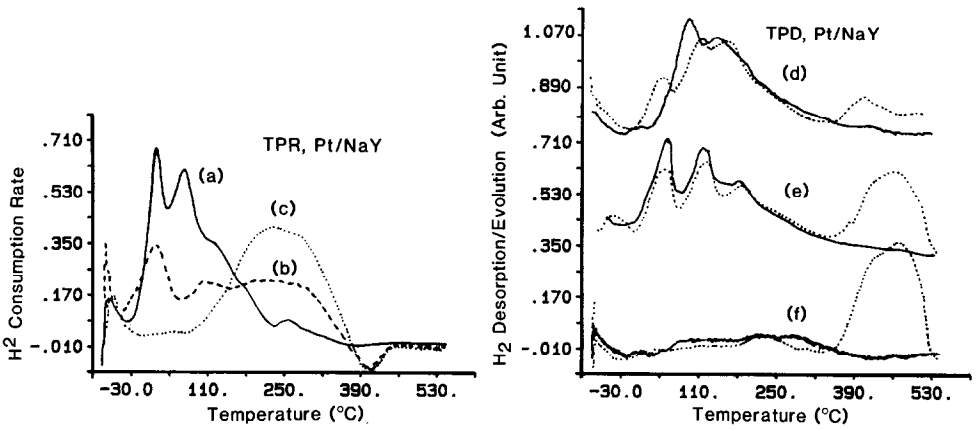

FIG. 1. TPR (curves a, b, c) and TPD (curves d, e, f) profiles of Pt/NaY samples, that had been calcined at 360, 450, or 550°C. (a) Pt/NaY(360); (b) Pt/NaY(450); (c) Pt/NaY(550); (d) Pt/NaY(360) after complete reduction (solid curve), and after interrupting reduction at 400°C (dotted curve); (e) as (d) for Pt/NaY(450); (f) as (d) for Pt/NaY(550).

reduction of Pt^{2+} ions was barely complete, the TPD profiles, shown by the dashed curves of Fig. 1d–1f were recorded. For these samples an additional desorption peak appears at T_{max} = 450°C, while the TPD profiles up to 350°C are similar to those for which reduction had not been interrupted at 400°C. It is interesting to note that the intensity of the additional TPD peak at 450°C increases with calcination temperature (in going from Fig. 1d to 1f). We have verified by mass spectrometry that the desorbed species is hydrogen only.

TPR spectra of Pt/FeNaY(360) and Pt/FeNaY(550) are displayed in Fig. 2, for 0.08 g of Pt/FeNaY(360). The reduction profiles of Pt/FeNaY(360) and Pt/NaY(360) are very similar in that the reduction of Pt^{2+} ions occurs at low temperatures, i.e., −15 to 150°C. A slight increase in the threshold reduction temperature by about 25°C is observed for Pt/FeNaY(360). The hydrogen consumption in TPR up to 550°C for Pt/FeNaY(360) is equivalent to the reduction of Pt^{2+} to Pt^0 and Fe^{3+} to Fe^{2+}. No further reduction of Fe^{2+} ions is observed by TPR. Upon calcination of the Pt/FeNaY to 550°C, some upward shift of the reduction temperature is again observed, as in Pt/NaY(550); in addition a new intense

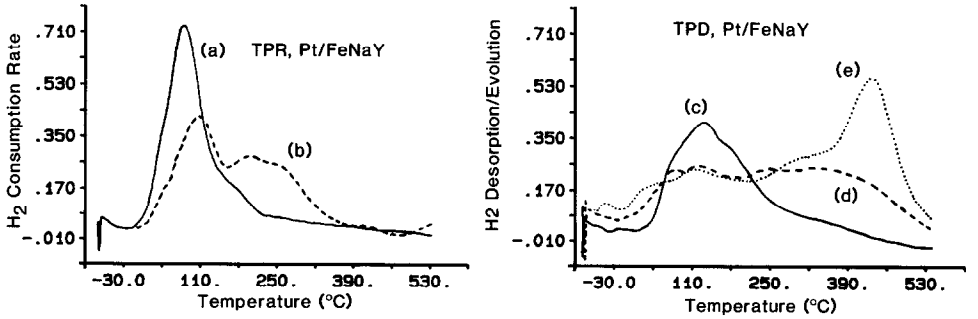

FIG. 2. TPR (curves a, b) and TPD (curves c, d) profiles of Pt/FeNaY samples, calcined at 360 or 550°C. (a) Pt/FeNaY(360); (b) Pt/FeNaY(550); (c) Pt/FeNaY(360) after complete reduction; (d) Pt/FeNaY(550) after complete reduction; (e) Pt/FeNaY(550) after interrupting reduction at 400°C.

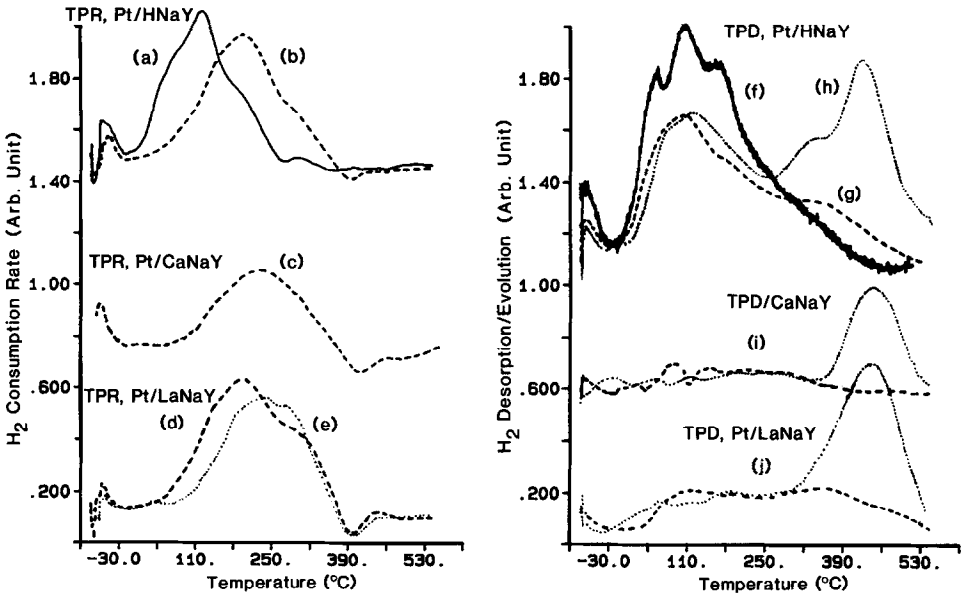

FIG. 3. TPR (curves a, b, c, d, e) and TPD (curves f, g, h, i, j) of Pt/NaY, Pt/HNaY, Pt/CaNaY, and Pt/LaNaY samples, calcined at 360 or 550°C. (a) Pt/HNaY(360); (b) Pt/HNaY(550); (c) Pt/CaNaY(550); (d) Pt/LaNaY(550); (e) Pt/NaY(550); (f) Pt/HNaY(360) after complete reduction; (g) Pt/HNaY(550) after complete reduction; (h) Pt/HNaY(550) after interrupting reduction at 400°C; (i) Pt/CaNaY(550) after complete reduction (dashed curve) and after interrupting reduction at 400°C (dotted curve); (j) Pt/LaNaY(550) after complete reduction (dashed curve) and after interrupting reduction at 400°C (dotted curve).

peak appears at approximately 100°C. Upon changing the Pt loading while keeping the Fe loading constant, only this peak at 100°C increases with Pt loading.

The TPD profiles of Pt/FeNaY(360) and Pt/FeNaY(550) are also shown in Fig. 2; the H/Pt ratios are 1.10 ± 0.10 and 0.72 ± 0.10, respectively. Obviously, the dispersion of Pt is markedly higher in Pt/FeNaY(550) than in Pt/NaY(550). The TPD profile was also recorded for the Pt/FeNaY(550) sample, whose TPR had been interrupted at 400°C, and is included in Fig. 2.

The TPR profiles for PT/HNaY(360), Pt/HNaY(550), Pt/CaNaY(550), and Pt/LaNaY(550) are shown in Fig. 3. The reduction temperature of Pt^{2+} ions in Pt/HNaY(360) and Pt/HNaY(550) increases with calcination temperature as in Pt/NaY. In general, the reduction temperature and profiles of the last three samples calcined at 550°C are very similar to those of Pt/NaY(550). The TPD profiles of Pt/HNaY(360), Pt/HNaY(550), Pt/CaNaY (550), and Pt/LaNaY(550) are also shown in Fig. 3, and their H/Pt ratios are 1.15 ± 0.10, 0.62 ± 0.10, 0.15 ± 0.10, and 0.28 ± 0.10, respectively.

3.2. *Infrared Spectra of Pt/NaY(550)*

The FTIR spectra of Pt/NaY(550) from 3500 to 4000 cm^{-1} are presented in Fig. 4. For the calcined Pt/NaY(550), there is a weak peak at 3750 cm^{-1} which is the vibrational peak of silanol group (*21, 22*). On the other hand, when the Pt/NaY(550) was reduced in H_2 in the TPR mode up to 400°C, a strong peak at 3645 cm^{-1} and a weak broad peak at 3550 cm^{-1} appear, as shown in Fig. 4b. It is believed that these two peaks are the vibrational peaks of hydroxyl groups, which are formed during the reduction of Pt with H_2. Dalla Betta and Boudart

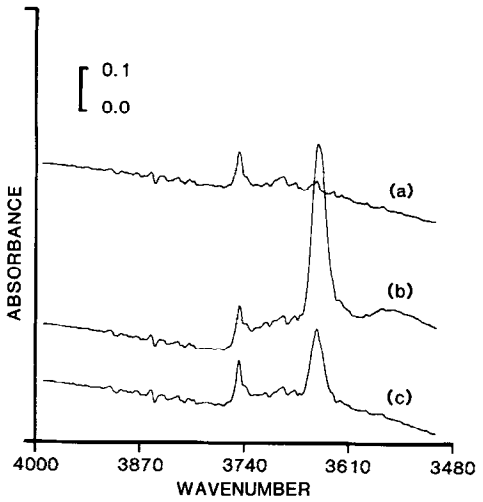

FIG. 4. IR Spectra of Pt/NaY(550). (a) After calcination; (b) after subsequent TPR up to 400°C; (c) after subsequent TPD up to 550°C.

(*3*) observed a peak at 3650 cm^{-1} after reduction of $Pt(NH_3)_4/CaNaY$ in H_2. The reduction of Cu/NaY at 200°C also generates peaks at 3650 and 3560 cm^{-1} as reported by Herman *et al.* (*23*). Further treatment in Ar in the TPD mode to 550°C decreases the 3650-cm^{-1} peak to one-third of its original intensity and causes the 3550-cm^{-1} peak to disappear (see Fig. 4c).

3.3. EXAFS Data Analysis

In order to investigate the chemical structure of platinum in various stages, X-ray absorption measurements at the Pt L_{III}-edge of Pt/Y zeolites was performed after ion exchange, calcination, and reduction at 360 and 550°C. The results of the data analysis are described below.

3.3.1. $Pt(NH_3)_4/FeNaY$. Plots of the $k^3 \cdot \chi(k)$ function vs k, where k is the photoelectron wave vector and $\chi(k)$ is the normalized EXAFS function, are shown in the left-hand section of Figs. 5a and 5b for $Pt(NH_3)_4/FeNaY$ and $Pt(NH_3)_4Cl_2$, respectively, dehydrated at 100°C *in vacuo*. Fourier transforms of $k^3 \cdot \chi(k)$, which are shown immediately to the right of the EXAFS plots, yield radial distribution functions $\psi(R)$, where R is the distance from the absorber atom. The Fourier transforms of the Pt L_{III} EXAFS were taken over the range of wave vectors 3.0 to 13.5 $Å^{-1}$ and have one peak at about 1.7 Å (before phase shift correction) for these two samples. The functions (solid curves) to the right of the Fourier transforms were obtained by inverting the transforms over restricted ranges of R, 1.5 to 2.4 Å. The functions (dashed curves) obtained in the curve fittings are also included in Fig. 5. Curve fitting gave rise to an average Pt^{2+}–N distance of 2.00 Å for both $Pt(NH_3)/FeNaY$ and $Pt(NH_3)_4Cl_2$, which is close to that of other ammine complexes characterized by X-ray crystallography (*24*). It is interesting to note that the local structures for the two systems, $Pt(NH_3)_4/FeNaY$ and $Pt(NH_3)_4Cl_2$, are virtually identical.

3.3.2. Calcined Pt/Y(360) and Pt/Y(550). EXAFS results are presented in Fig. 5 for the calcined samples Pt/NaY(360), Pt/NaY(550), Pt/FeNaY(360), Pt/FeNaY (550), and Pt/LaNaY(550). Plots of the $k^3 \cdot \chi(k)$ vs k functions are displayed in the left part of Figs. 5c–5g. The Fourier transforms of these EXAFS data were taken over a range of k from 3 to 14.2 $Å^{-1}$. In general, there are two peaks at 1.7 and 2.8 Å (before phase correction) in the radial distribution functions, as shown in the second column of Fig. 5. The inverse transforms were taken over the ranges of R from 1.0 to 2.7 Å for the first peak, yielding $k^3 \cdot \chi_1(k)$, and 1.8 to 3.6 Å for the second peak, yielding $k^3 \cdot \chi_2(k)$; they are shown separately as the solid curves in the right-hand section of Fig. 5. Note that the peak intensity at R = 2.8 Å (before phase correction) for Pt/NaY(550) and Pt/LaNaY(550) is exceptionally high (see below).

The peak at R = 1.7 Å (uncorrected), whose inversed Fourier transform is similar to that of PtO_2, is assigned to Pt^{2+}–O^{2-}, which is reasonable for calcined samples. After curve fittings, shown as dashed curves, the Pt–O distance and coordination

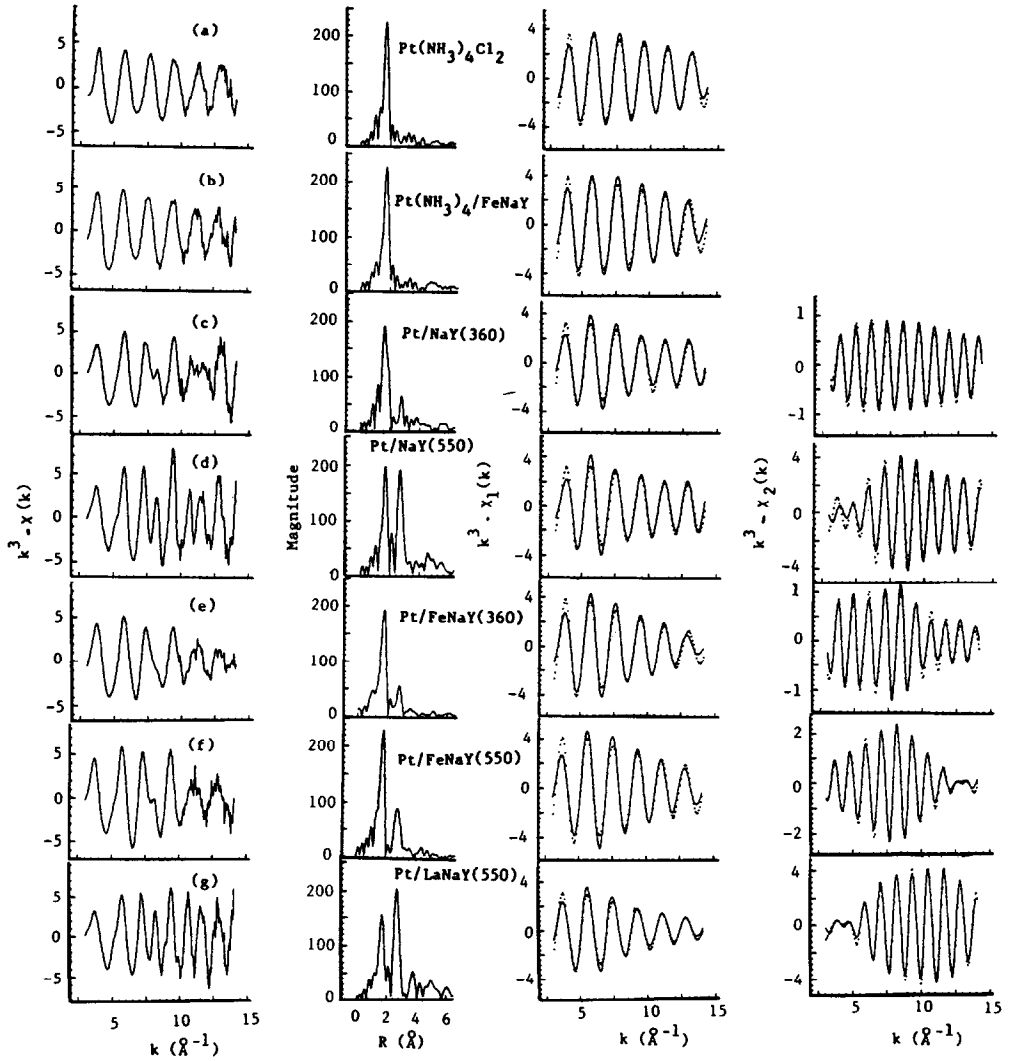

FIG. 5. k^3-weighted EXAFS function (first column), Fourier transforms of $k^3 \cdot \chi(k)$ functions (second column), and inversed Fourier transforms of first peak (third column) and second peak (fourth column) of radial distribution functions for (a) $Pt(NH_3)_4Cl_2$, (b) $Pt(NH_3)_4$/FeNaY calcined, (c) Pt/NaY(360), (d) Pt/NaY(550), (e) Pt/FeNaY(360), (f) Pt/FeNaY(550), and (g) Pt/LaNaY(550).

numbers are obtained, and the results are listed in Table 2. The inverse Fourier transforms of the second peak at R = 2.8 Å (uncorrected) for Pt/NaY(360), Pt/FeNaY(360), and Pt/FeNaY(550) can be attributed to Al (and Si) and/or Fe as backscattering atoms and fitted with one-term (Al/Si) and two-term (Al/Si and Fe) models, respectively. The heavier elements Pt and La in Pt/NaY(550) and Pt/LaNaY(550) must, however, be included as additional backscattering atoms in the curve fittings of the inverse Fourier transforms of the second peak at R = 2.8 Å (uncorrected). The bond distances between absorber atoms and second shell coordination atoms are also included in Table 2. Second neighbor shells of framework oxygen, aluminum, and silicon atoms have also been observed by EXAFS in dehydrated Co/NaA and Mn/NaA (*25, 26*).

We have also used $k \cdot \chi(k)$ as an EXAFS

TABLE 2

Structural Parameters of Calcined Pt/Y Zeolites[a]

Catalysts	Coord. Atom	Bond Dist.	Coord. Number
$Pt(NH_3)_4Cl_2$	Pt–N	2.01 ± 0.02 Å	4
$Pt(NH_3)_4$/FeNaY	Pt–N	2.00	4
PtO_2	Pt–O	2.00	6
Pt/NaY(360)	Pt–O	2.03	3.1
	Pt–Al(Si)	3.16	
Pt/NaY(550)	Pt–O	2.05	3.3
	Pt–Al(Si)	3.20	
	Pt–Pt	2.95	
Pt/FeNaY(360)	Pt–O	2.03	3.3
	Pt–Al(Si)	3.21	
	Pt–Fe	3.00	
Pt/FeNaY(550)	Pt–O	2.04	3.9
	Pt–Al(Si)	3.24	
	Pt–Fe	3.00	
Pt/LaNaY(550)	Pt–O	2.05	2.8
	Pt–Al(Si)	3.15	
	Pt–La	2.98	
	Pt–Pt	3.00	

[a] Structural parameters are derived from k^3-weighted EXAFS functions.

function to analyze $Pt(NH_3)_4$/FeNaY and calcined samples. There is a strong artifact peak at R = 1.0 to 1.2 Å, which complicates the Fourier transforms of $k \cdot \chi(k)$ functions and their further analysis. However, the results are identical to those derived from k^3-weighted EXAFS functions.

3.3.3. Reduced Pt/Y(360) and Pt/Y(550). Similar plots, i.e., $k^3 \cdot \chi(k)$ EXAFS, their corresponding Fourier transforms and inverse transforms, are shown in Figs. 6b–6g for reduced Pt/NaY(360), Pt/NaY(550), Pt/FeNaY(360), Pt/FeNaY(550), Pt/HNaY (550), and Pt/LaNaY(550). The Fourier transforms of the reduced Pt/Y catalysts were taken over in the range of k from 3.0 to 15.0 Å. There is only one peak at about 2.5 Å (before phase correction) in the radial distribution functions of these reduced catalysts. The inverse transforms were taken over the range of R from 1.4 to 3.8 Å. The results of the data analysis are listed in Table 3, using 2.5-μm Pt aggregates mixed with NaY as reference compound (see Fig. 5a) to obtain the coordination numbers of Pt in reduced Pt/Y(360) and Pt/Y(550). We were unable to obtain the distance between Pt^0 atoms and oxygen atoms of the support when using the $k^3 \cdot \chi(k)$ EXAFS functions. On the other hand, use of the k^1-, instead of k^3-, weighted EXAFS functions to emphasize the low-Z elements as backscattering atoms enabled us to find that the distance for Pt^0–O^{2-} is 2.65 Å, which is consistent with data reported for reduced Pt/Al_2O_3 catalysts (*27*).

4. DISCUSSION

4.1. Pt/NaY(360) and Pt/NaY(550)

The variations in the reduction temperature of Pt^{2+} ions and in the dispersion of Pt particles with calcination temperature (see TPR and TPD in Figs. 1a to 1f) have been discussed before in some detail (*12*). In order to correlate with the FTIR spectra, TPR/TPD, and EXAFS data described in Section 3, the conclusions derived from Fig. 1 are briefly summarized below.

(i) As $Pt(NH_3)_4$/NaY is calcined at low temperatures (e.g., 360°C) to remove NH_3 ligands, the majority of Pt^{2+} ions are in the

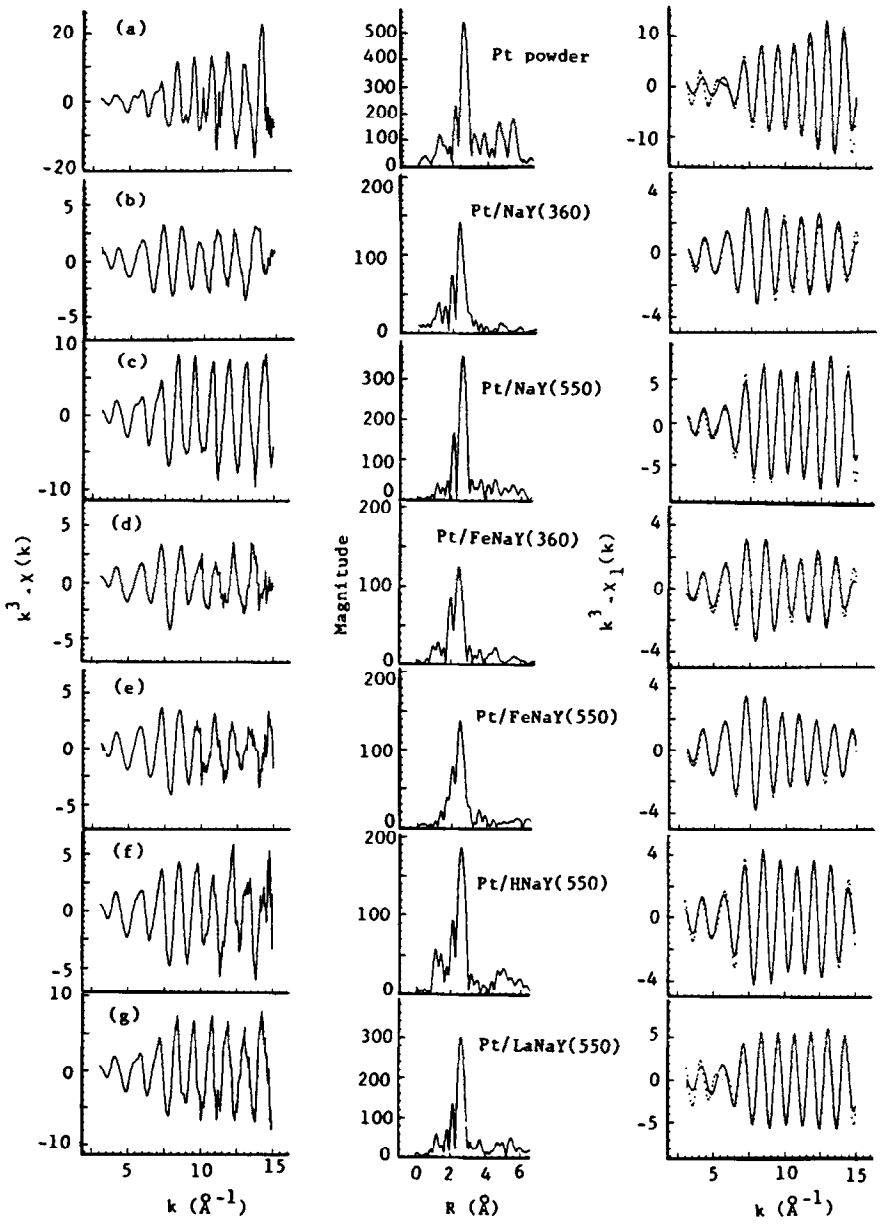

FIG. 6. k^3-weighted EXAFS functions (first column), Fourier transforms of $k^3 \cdot \chi(k)$ functions (second column), and their inversed Fourier transforms of radial distribution functions between R = 1.4 and 3.8 Å (third column) for (a) Pt powder (2.5 μm) mixed with NaY and reduced, (b) Pt/NaY(360), (c) Pt/NaY(550), (d) Pt/FeNaY(360), (e) Pt/FeNaY(550), (f) Pt/HNaY(550), and (g) Pt/LaNaY(550).

supercages where Pt^{2+} ions are accessible to H_2 molecules and easily reduced at low temperatures forming small particles with a dispersion of near 100%. Gallezot *et al.* showed that Pt particles are small as 6–13 Å are formed in Pt/NaY zeolites that were calcined and reduced at 300°C (*4*). There is a general consensus that these small Pt particles are located in the supercages.

(ii) When the calcination temperature is raised to 450°C, about 50% of the Pt^{2+} ions migrate to sodalite cages (cf. Fig. 1, curve

TABLE 3

Structural Parameters of Reduced Pt/Y Zeolites

Catalysts	E_0 (eV)	σ	r_{Pt-Pt}[a] (Å)	N_{Pt-Pt}[b]
Pt powder (2.5 μm)/NaY	4.05	0.057	2.76 ± 0.02	12
Pt/NaY(360)	0.31	0.079	2.64	7.7
Pt/NaY(550)	3.86	0.063	2.74	11.5
Pt/FeNaY(360)	1.40	0.082	2.64	7.3
Pt/FeNaY(550)	1.89	0.084	2.67	7.7
Pt/HNaY(550)	2.69	0.075	2.69	9.2
Pt/LaNaY(550)	5.76	0.069	2.74	10.4

[a] Best fitted data based on theory.
[b] Derived from $\ln[A/A_r] = \ln[NR_r/N_rR] - 2k^2(\sigma^2 - \sigma_r^2)$.

(b)). The kinetic diameter of the H_2 molecule (2.9 Å) is larger than that of the O_6 rings (2.2 Å) (*4*, *28*), and the Pt^{2+} ions in sodalite cages are more stable. They, therefore, require a higher reduction temperature than the Pt^{2+} ions which remain in supercages and are reduced in the same temperature region as Pt^{2+} in Pt/NaY(360). This leads to an interesting consequence for the ultimate size of the Pt particles: The small Pt particles in the supercages which are formed first act as nucleation sites to trap the Pt atoms coming out of the sodalite cages. Eventually, the growing Pt particles will protrude into adjacent supercages, becoming larger than the dimension of the supercage, but still remaining inside the zeolite. A Pt dispersion near 60% is calculated from the integrated TPD of Pt/NaY(450) in Fig. 1e (solid curve).

(iii) If $Pt(NH_3)_4$/NaY is calcined at higher temperatures (e.g., 550°C), most Pt^{2+} ions migrate to sodalite cages and can be reduced only at higher temperatures. Using powder X-ray diffraction, Gallezot *et al.* found that more than 90% of the Pt^{2+} ions are at SI′ sites in Pt/HNaY calcined at 600°C (*4*). When the temperature is raised from 400 to 550°C, the Pt atoms, which have been reduced below 400°C, will leave the sodalite cages, traversing the O_6 rings, and then the channels and supercages. Due to low concentration or total absence of Pt clusters or other adequate nucleation sites in the supercages, the Pt atoms will migrate all the way to the external surface of the zeolite cyrstals to form large particles. Accordingly, a low-Pt dispersion is found for Pt/NaY(550) (see Fig. 1f solid curve). An electron micrograph of Pt/NaY(550) taken by the HRTEM (Hitachi 9000) and shown in Fig. 7 reveals indeed large Pt particles on the external surface of the zeolite crystal.

The migration of metal cations in X and Y zeolites from accessible cages to "hidden" sites has been reported for numerous metal cations. Data on the cation locations in extra framework positions have been compiled by Mortier (*29*). The strong preference of multivalent cations with high charge density for type I and I′ sites after dehydration is probably a consequence of the high density of the negative charge around hexagonal prisms. Particularly for Y-type zeolite, the negative charge density in hexagonal prisms is higher than that at any other sites of the zeolite. Indeed, a Monte Carlo simulation shows that 99% of the hexagonal prisms contain two or more aluminum atoms for Y zeolites with a Si/Al ratio of 2.49 (*30*). This exceptionally high Coulomb interaction and the steric difficulty of admitting dihydrogen molecules through O_6 rings result in the low reducibility of cations in these positions. A decreased reducibility of metal ions has also been observed for alumina-supported metals, e.g., Pt or Re (*31*, *32*); in these systems

FIG. 7. HRTEM of Pt/NaY(550) with magnitude 1,000,000.

a high interfacial interaction between supported and supporting oxide is very likely, possibly accompanied by some atomic reorganizations.

When temperature-programmed reduction of Pt/NaY(360), Pt/NaY(450), or Pt/NaY(550) is interrupted at 400°C, a characteristic peak is observed at 450°C in the following TPD spectrum (see dotted lines in Figs. 1d–1f). The area under this peak increases with calcination temperature. We conclude that this peak area is roughly proportional to the number of Pt^{2+} ions in sodalite cages after calcination. The reduction of Pt^{2+} ions by H_2 leads to the formation of protons which are associated to matrix O^{2-} ions as OH^- groups:

$$(-T-O)_2Pt + H_2 \rightarrow 2(-T-O-H) + Pt^0 \quad (1)$$

where T is Al or Si. The generation of these hydroxyl groups due to reduction at 400°C has been detected by IR bands at 3550 and 3645 cm^{-1}, as shown in Fig. 4b. Further thermal treatment up to 550°C in Ar causes a decrease in intensity of the IR band at 3645 cm^{-1} and the disappearance of the 3550-cm^{-1} band. This strongly suggests that the evolved hydrogen at 450°C is due to the reverse reaction of Eq. (1). We confirmed this conclusion by reoxidizing two Pt/NaY(550) samples and measuring the oxygen uptake. One sample had been reduced up to 550°C, the other sample reduction was interrupted at 400°C, and hydrogen evolution in the TPD mode was registered including the peak at 450°C. It was found that the oxygen uptake by the latter sample is about 66% lower in accordance with the model that the H_2 evolution at 450°C (at low H_2 pressure) is due to reoxidation of Pt^0 by protons. No such reoxidation by H^+ takes place under TPR conditions (high H_2 pressure), when Pt atoms migrate out of the sodalite cages. Recently, the reoxidation of metal atoms by hydroxyl groups in small cages of zeolite Y has also been verified for Ni/NaY (*48*).

Previously, we had suggested that such a peak might also be due to the desorption of hydrogen adsorbed on Pt atoms in sodalite cages (*14*). This possibility has now been ruled out by the following observations: (i) The consumption of hydrogen during TPR of Pt/NaY(550) is equivalent to two H atoms per Pt^{2+} ion. If metal reduction is coupled with hydrogen adsorption, the total hydrogen consumption under the TPR profiles would be near three H atoms per Pt^{2+} ion, and (ii) no additional hydrogen adsorption was detected during the cooling process, after interruption of the TPR of Pt/NaY(550) at 400°C. Our material balance thus shows that Pt^0 atoms in sodalite cages adsorb hydrogen neither at high nor at room temperature. Gallezot *et al.* (*4*) discussed four possible causes of the failure of such Pt^0 atoms to chemisorb hydrogen, including the necessity of having at least a pair of two Pt atoms to dissociate a H_2 molecule. Our EXAFS data (vide infra) show that there are actually two Pt atoms in some sodalite cages; we therefore assume that the H adsorption is thermodynamically unfavorable on these Pt^0 atoms at high temperatures, while H_2 molecules cannot enter through the narrow windows at low temperatures in the absence of sufficient lattice vibration.

The TPD data in Fig. 1 also suggest that the reactivity of very small Pt particles in Pt/NaY(360) with hydroxyl groups is negligible. Based on the data presented above, the hydrogen evolution at high temperatures in Figs. 1d–1f (dashed curves) can be regarded as a yardstick for the presence of Pt^0 atoms in sodalite cages. However, the amount of hydrogen evolved at high temperatures is about 25% less than the amount calculated from Eq. (1) and the number of Pt^0 atoms in sodalite cages. It suggests that some Pt atoms may escape through the O_6 rings instead of reacting with the hydroxyl groups.

The EXAFS data analysis of calcined Pt/NaY(360), showing bonding of Pt^{2+} ions with three oxygen at 2.03 Å and tetrahedral atoms (Al or Si) at 3.20 Å, suggests that Pt^{2+} ions are at cationic exchange sites.

The result of our curve fittings (dashed

curve) that in Pt/NaY(550) Pt is the backscattering atom at a distance of 3.20 Å from the absorber suggests that there are at least two Pt atoms in some sodalite cages. Considering the composition of our Pt/NaY with a metal load of about 0.7 Pt/sodalite cage, the distribution of $Pt(NH_3)_4^{2+}$ complexes in the zeolite crystal is probably not homogeneous. This might be caused by an inhomogeneous distribution of Al in the zeolite. Thermal rearrangement of Pt^{2+} ions might result in a situation such that two Pt^{2+} ions are present in the same sodalite cage.

The coordination numbers of Pt in reduced Pt/NaY(360) and Pt/NaY(550) indicate that the average particle size of the Pt particles in Pt/NaY(550) is much larger, in agreement with the dispersion data and the particle formation mechanisms described earlier. The shrinkage of the Pt–Pt bond distance in the small particles in the absence of H_2 is noteworthy; this bond shortening was also reported by others for Pt (*33, 34*) and for Rh in Rh/X and Rh/Y zeolites (*19, 35*).

4.2. Pt/FeNaY(360) and Pt/FeNaY(550)

Reduction of Pt^{2+} ions in Pt/FeNaY(360) occurs in the same temperature region as in Pt/NaY(360), which suggests that the majority of Pt^{2+} ions are also in the supercages. The Fe^{2+} cations, which are incorporated into zeolites by ion exchange, are oxidized to Fe^{3+} during the calcination step. Mössbauer data show that these ions are largely located in the sodalite cages (*36*). Since the reduction of Fe^{3+} in Fe/NaY occurs at T_{max} = 350°C (*17*), it is obvious that platinum catalyzes the reduction of Fe^{3+} to Fe^{2+}, as shown in Fig. 2a.

For the Pt/FeNaY(550), we would expect that most Pt^{2+} and Fe^{3+} cations would migrate to sodalite cages and are reduced above 100°C, as mentioned above. However, a strong hydrogen consumption peak appears near 100°C, which might be due to the reduction of Pt^{2+} ions located in accessible positions rather than the reduction of Fe^{3+} cations because of the higher reduction potential of the Pt^{2+} ion.

The migration of cations from supercages to sodalite cages and hexagonal prisms is dependent on the dehydration temperature and the period of thermal treatment. The collected data of dehydrated Y-type zeolites with multivalent metal cations indicate that the total charges of these multivalent cations in sodalite cages and hexagonal prisms are in the range from 24 to 32 per unit cell for most metal cations exchanged into Y-type zeolites (*29*). The total charge of Pt and Fe in Pt/FeNaY is about 38. Since the Fe^{3+} ions have a high charge density, they are most favorably located in small cages. When Pt^{2+} ions also migrate to sodalite cages at high temperatures, an equilibrium or saturation state will be attained, and the rest of the Pt^{2+} ions remain in the supercages where they are identified by the strong TPR peak at low temperatures, as shown in Fig. 2b.

The EXAFS data of calcined Pt/FeNaY(550) are in agreement with this site blocking model. The Fe^{3+} ion in the sodalite cage renders access of no more than one Pt^{2+} ion—at the most—to the same sodalite cage. As expected, due to the low backscattering amplitudes of Fe, Al, and Si atoms, the peaks at 2.8 Å (uncorrected) in the radial distribution function of calcined Pt/FeNaY(550) are weaker than those observed for Pt/NaY(550), since the sodalite cages are now blocked by Fe^{3+} ions.

The TPD profile of Pt/FeNaY(550) for which TPR was interrupted at 400°C also possesses a hydrogen evolution peak at 450°C, which implies that some Pt^{2+} ions are also in the sodalite cages after calcination at 550°C. Therefore the process for the formation of Pt particles should be very similar to that observed in Pt/NaY(450) where Pt^{2+} ions are distributed over both supercages and sodalite cages. The TPD result indicates that the dispersion of Pt particles is 72%. The low coordination number of Pt in Pt/FeNaY(550) derived from EXAFS, likewise, suggests formation of small Pt particles.

Previously, we found a direct bonding interaction between Rh atoms and Cr ions

in reduced Rh/CrNaY (*19*). From the present EXAFS data on the reduced Pt/FeNaY, we were not able to derive that a similar interaction exists between Pt atoms and Fe^{2+} ions. However, the slower decrease in Pt dispersion for Pt/FeNaY in comparison to Pt/NaY, upon heating the samples in H_2 for many hours, provides evidence for "chemical anchoring" of *Pt particles* by Fe ions (*13*). It has also been reported that Fe^{2+} ions are in supercages after reduction of FeNaY (*37*). From studies of the proton spin relaxation time, it has been suggested that Pt atoms which have not agglomerated to particles preferentially associate themselves with Fe^{3+} (*38, 39*).

4.3. Pt/LaNaY(550) and Pt/CaNaY(550)

With Ca^{2+} and La^{3+} as auxiliary cations, the TPR in Fig. 3 shows that the reduction profiles are surprisingly similar to that of Pt/NaY(550). The total charge of Ca^{2+} and Pt^{2+} in Pt/CaNaY is about 30. Ca^{2+} and Pt^{2+} cations are probably located in the sodalite cages and/or hexagonal prisms after calcination at 550°C. Therefore, the reduction behavior and particle formation would follow the course of Pt/NaY(550) to give large Pt particles, and in fact the small TPD peaks give a low H/Pt ratio (see Fig. 3).

However, for Pt/LaNaY(550), the total charges of Pt^{2+} and La^{3+} cations add up to about 48. If the La^{3+} ions effectively block the small cages, it would leave a portion of Pt^{2+} ions in supercages such that Pt^{2+} ions can be reduced at about 100°C to act as nucleation sites as observed for Pt/FeNaY(550). However, in the reduction profile of Pt/LaNaY(550) the area in the low temperature region is only slightly larger than that in Pt/NaY(550). For comparison, the TPR of Pt/NaY(550) is also included in Fig. 3e. The results suggest that the fraction of Pt^{2+} ions in supercages is very small.

Two possibilities are mentioned to rationalize this observation. (i) The La^{3+} cations might be hydrolyzed to form $[La(OH)La]^{5+}$ dimers in sodalite cages (*40*). This would lead to a decrease in the total formal charge during the dehydration treatment prior to ion exchange with $Pt(NH_3)_4Cl_2$. Two Pt^{2+} ions may then migrate to those sodalite cages that do not contain lanthanum cations. (ii) It has been suggested that (Ni–O–La)- and (Cu–O–Ce)-type associations might be present in zeolites containing these multivalent cations (*41, 42*). This will stabilize the Ni^{2+} and Cu^{2+} ions and decrease their reducibility. The formation of (Pt–O–La) adducts might also lead to a stabilization of the Pt^{2+} cations.

The EXAFS analysis of calcined Pt/LaNaY(550) suggests that both Pt and La are the backscattering atoms giving rise to the second peak at 2.8 Å in the Fourier transform function, as shown in Fig. 6. It seems that rationalizations given above are quite reasonable; some support for this view is found by the radial electron distribution results which show that $[La(OH)La]^{5+}$ dimers are formed in sodalite cages (*43*). These species have been assumed to stabilize the zeolite structure of cracking catalysts (*44*). Basically, the formation of Pt particles is very similar to what we have seen in Pt/NaY(550). The coordination number derived from the EXAFS of reduced Pt/LaNaY(550) also suggests the formation of large Pt particles.

4.4. Pt/HNaY(360) and Pt/HNaY(550)

The reduction of Pt^{2+} ions in Pt/HNaY(360) is complete at 200°C with T_{max} = 120°C which is higher than that for nonacidic samples calcined at 360°C. The increase in the threshold reduction temperature is probably related to the redox equilibrium, which is also observed in the reduction of Ni^{2+} ions in acidic zeolites (*45, 46*). On the other hand, the reduction temperature and T_{max} = 200°C of Pt^{2+} ions in Pt/HNaY(550) is lower than that in Pt/NaY(550) because at 550°C some Pt^{2+} ions remain in the supercages (see below).

For Pt/HNaY(550), the TPD profile (dashed curve of Fig. 3h) indicates that Pt^{2+}

ions are, again, distributed between supercages and sodalite cages. The peak area in the high temperature region (i.e., 350 to 550°C) indicates that at least 30% of the Pt^{2+} ions are located in the sodalite cages. Clearly, the formation processes for the Pt particles in Pt/HNaY(550) should be very similar to that in Pt/NaY(450) with sizes larger than the dimension of the supercage. In fact, the dispersion of Pt particles calculated from the TPD (solid curve of Fig. 3g) is 62%. The coordination number of Pt in Pt/HNaY(550) is slightly larger than that in the samples that were treated at 360°C, but smaller than that in Pt/NaY(550). Possible causes for some Pt^{2+} ions to remain in the supercages of Pt/HNaY(550) include the following:

(i) Strong bonding of protons with the O_3 atoms may inhibit the migration of Pt^{2+} ions to type I′ sites.

(ii) During the deammination in preparing HNaY, some dealumination may occur leading to the octahedrally coordinated Al in the sodalite cages (*47*). This would result in blocking of the sodalite cages, and the Pt^{2+} ions would remain in the supercages, as was observed for Pt/FeNaY(550).

5. CONCLUSIONS

This study leads to the following conclusions:

(i) The formation of Pt particles of various sizes located either inside or outside Y-type zeolites is mainly determined by the distribution of Pt^{2+} ions between supercages and sodalite cages prior to reduction. This distribution can be controlled by the calcination temperature.

(ii) The number of Pt^{2+} ions which have migrated to sodalite cages can be estimated semiquantitatively from the evolution of hydrogen in TPD at T_{max} = 450°C, after interruption of the temperature-programmed reduction at 400°C.

(iii) The presence of sufficient multivalent cations (e.g., Fe^{2+}, Ca^{2+}, and La^{3+}) in NaY results in blocking of hexagonal prisms and/or sodalite cages for Pt^{2+} ions. These Pt^{2+} ions then remain in supercages even at high T_c. They are reduced at low temperatures and then can act as nucleation sites to trap Pt^0 atoms escaping from sodalite cages at high temperatures. This may lead to the formation of Pt particles somewhat larger than the dimension of the supercage, but still remaining inside the zeolite.

(iv) If the number of multivalent cations is not sufficient to block the small cages, virtually all Pt^{2+} ions will ultimately be located in sodalite cages at high T_c. A high reduction temperature is then required, and migration of the reduced platinum to the external surface of the zeolite crystals will lead to the formation of large Pt particles.

(v) At high T_c, two Pt^{2+} ions at the most will be located in the same sodalite cage in Pt/NaY; the presence of such pairs is suggested by the EXAFS data.

ACKNOWLEDGMENTS

We gratefully acknowledge support from the U.S. Department of Energy under Contracts DE-ACO2-84ER13157 and DE-FG02-87ERA3654. The authors are indebted to Johnson Matthey Inc. for tetrammine platinous chloride and to Dr. J. P. Zhang for his invaluable assistance in carrying out the high-resolution electron microscopic study.

REFERENCES

1. Minachev, Kh. M., and Isakov, Ya. I., *in* "Zeolite Chemistry and Catalysis" (J. A. Rabo, Ed.), Vol. 171, p. 552. ACS monograph, 1976.
2. Rabo, J. A., Schomaker, V., and Pickert, P. E., *in* "Proceedings, 3rd International Congress on Catalysis, Amsterdam, 1964" (W. M. H. Sachtler, *et al.*, Eds.), Vol. 2, p. 1264. North-Holland, Amsterdam, 1965.
3. Dalla Betta, R. A., and Boudart, M., "Proceedings, 5th International Congress on Catalysis, Palm Beach, 1972" (J. W. Hightower, Ed.), p. 1329. North-Holland, Amsterdam, 1973.
4. Gallezot, P., Alarcon-Diaz, A., Dalmon, J.-A. Renouprez, A. J., and Imelik, B., *J. Catal.* **39,** 334 (1975).
5. Jacobs, P. A., *in* "Metal Clusters in Catalysis" (B. C. Gates, *et al.*, Ed.), p. 357. Elsevier, Amsterdam, 1986.
6. Kleine, A., Ryder, P. L., Jaeger, N., and Schulz-Ekloff, G., *J. Chem. Soc. Faraday Trans. 1* **82,** 205 (1986).

7. Delafosse, D., *J. Chim. Phys.* **83,** 791 (1986).
8. Gallezot, P., and Bergeret, G., *in* "Catalyst Deactivation" (E. E. Peterson and A. T. Bell, Eds.), p. 263. Dekker, New York, 1987.
9. Felthouse, T. R., and Murphy, J. A., *J. Catal.* **98,** 411 (1986).
10. Exner, D., Jaeger, N. I., Moller, K., Nowak, R., Schrubbers, H., Schulz-Ekloff, G., and Ryder, P., *in* "Metal Microstructures in Zeolites" (P. Jacobs, *et al.*, Eds.), p. 205. Elsevier, Amsterdam, 1982.
11. Ward, J., *in* "Applied Industrial Catalysis" (B. Leach, Ed.), Vol. 3, p. 271. Academic Press, San Diego, 1984.
12. Tzou, M. S., and Sachtler, W. M. H., *in* "Catalysis 1987" (J. W. Ward, Ed.) p. 233. Elsevier, Amsterdam, 1988.
13. Tzou, M. S., Jiang, H. J., and Sachtler, W. M. H., *Appl. Catal.* **20,** 231 (1986).
14. Tzou, M. S., Jiang, H. J., and Sachtler, W. M. H., *React. Kinet. Catal. Lett.* **35,** 207 (1987).
15. Tri, T. M., Massardier, J., Gallezot, P., and Imelik, B., *in* "Proceedings, 7th International Congress on Catalysis, Tokyo, 1980" (T. Seiyama and K. Tanabe, Eds.), p. 266. Elsevier, Amsterdam, 1981.
16. Naccache, C., Kaufherr, N., Dufaux, M., Pandiera, J., and Imelik, B., *Amer. Chem. Soc. Symp. Ser.* **40,** 538 (1977).
17. Park, S. H., Tzou, M. S., and Sachtler, W. M. H., *Appl. Catal.* **24,** 85 (1986).
18. Tessier-Youngs, C., Correa, F., Pioch, D., Burwell, R. L., and Shriver, D. F., *Organometallics* **2,** 898 (1983).
19. Tzou, M. S., Teo, B. K., and Sachtler, W. M. H., *Langmuir* **2,** 773 (1986).
20. (*a*) Teo, B. K., Antonio, M. R., and Averill, B. A., *J. Amer. Chem. Soc.* **105,** 3751 (1983); (*b*) Teo, B. K., "EXAFS: Basic Principles and Data Analysis." Springer-Verlag, Heidelberg, 1986.
21. Ward, J., *in* "Zeolite Chemistry and Catalysis" (J. A. Rabo, Eds.), Vol. 171, p. 118. ACS monograph, 1976.
22. Dalla Betta, R. A., Garten, R. L., and Boudart, M., *J. Catal.* **41,** 40 (1976).
23. Herman, R. G., Lunsford, J. H., Beyer, H., Jacobs, P. A., and Uytterhoeven, J. B., *J. Phys. Chem.* **79,** 2388 (1975).
24. Bell, J. D., Bowles, J. C., Cumming, H. J., Hall, D., and Holland, R. V., *Acta Crystallogr. B* **32,** 634 (1976).
25. Morrison, T. I., Iton, L. E., Shenoy, G. K., Stucky, G. D., Suib, S. L., and Reis, A. H., *J. Chem. Phys.* **73,** 4705 (1980).
26. Morrison, T. I., Iton, L. E., Shenoy, G. K., Stucky, G. D., and Suib, S. L., *J. Chem. Phys.* **75,** 4086 (1981).
27. Koningsberger, D. C., and Sayers, D. E., *Solid State Ionics* **16,** 23 (1981).
28. Breck, D. W., "Zeolite Molecular Sieves: Structure, Chemistry and Use," p. 636. Wiley, New York, 1974.
29. Mortier, W. J., "Compilation of Extra Framework Sites in Zeolites." Butterworths, Guildford, 1982.
30. Aparicio, L. M., Dumesic, J. A., Fang, S.-M., Long, M. A., Ulla, M. A., Millman, W. S., and Hall, W. K., *J. Catal.* **104,** 381 (1987).
31. Yao, H. C., Sieg, M., and Plummer, H. K., Jr., *J. Catal.* **59,** 365 (1979).
32. Augustine, S., and Sachtler, W. M. H., *J. Catal.*, submitted.
33. Moraweck, B., and Renouprez, A. J., *Surf. Sci.* **106,** 35 (1981).
34. Boudart, M., Samant, M. G., and Ryoo, R., *Ultramicroscopy* **20,** 125 (1986).
35. Denley, D. R., Raymond, R. H., and Tang, S. C., *J. Catal.* **87,** 414 (1984).
36. Garten, R. L., Delgass, W. N., and Boudart, M., *J. Catal.* **18,** 90 (1970).
37. Pearce, J., Mortier, W. J., Uytterhoeven, J. B., and Lunsford, J. H., *J. Chem. Soc. Faraday Trans. 1* **77,** 937 (1981).
38. Wirkler, H., Ebert, A., and Riedel, W., *Surf. Sci.* **50,** 565 (1975).
39. Heyer, W., and Winkler, H., *Z. Phys. Chem. Leipzig* **258,** 692 (1977).
40. Smith, J. V., Bennett, J. M., and Flanigen, E. M., *Nature (London)* **215,** 241 (1967).
41. Conesa, J. C., and Soria, J., *J. Chem. Soc. Faraday Trans. 1* **75,** 423 (1979).
42. Briend-Faure, M., Jeanjean, J., Delafosse, D., and Gallezot, P., *J. Phys. Chem.* **84,** 875 (1980).
43. Mauge, F., Gallezot, P., Courcelle, J.-C., Engelhard, P., and Grosmangin, J., *Zeolites* **6,** 261 (1986).
44. Rabo, J. A., Angell, C. L., and Schomaker, V., *in* "Proceedings, 4th International Congress on Catalysis, Moscow, 1968" (B. A. Kazansky, Ed.), paper 54. Adler, New York, 1968.
45. Mirodatos, C., and Barthomeuf, D., *in* "Proceedings, Internal. Symp. Zeolite Catal.," p. 241. Siofok, Hungary, 1985.
46. Suzuki, M., Tsutsumi, K., and Takahashi, H., *Zeolites* **2,** 51 (1982).
47. Shannon, R. D., Gardner, K. H., Staley, R. H., Bergeret, G., Gallezot, P., and Auroux, A., *J. Phys. Chem.* **89,** 4778 (1985).
48. Jiang, H. J., Tzou, M. S., and Sachtler, W. M. H., *Catal. Lett.*, in press.